Nr. 24
11. June 2016

Leopold-Franzens-Universität Innsbruck

Preprint-Series: Department of Mathematics - Applied Mathematics

Compressed sensing and sparsity in photoacoustic tomography

M. Haltmeier, T. Berer, S. Moon and P. Burgholzer

APPLIEDMATHEMATICS

Technikerstraße 13 - 6020 Innsbruck - Austria
Tel.: +43 512 507 53803 Fax: +43 512 507 53898
https://applied-math.uibk.ac.at

Compressed sensing and sparsity in photoacoustic tomography

Markus Haltmeier[1], Thomas Berer[2], Sunghwan Moon[3] and Peter Burgholzer[2,4]

[1] Department of Mathematics, University of Innsbruck, Technikerstrasse 13, A-6020 Innsbruck, Austria

[2] Research Center for Non-Destructive Testing (RECENDT), Altenberger Straße 69, 4040 Linz, Austria.

[3] Department of Mathematical Sciences, Ulsan National Institute of Science and Technology, Ulsan 44919, Republic of Korea

[4] Christian Doppler Laboratory for Photoacoustic Imaging and Laser Ultrasonics, Altenberger Straße 69, 4040 Linz, Austria.

E-mail: `markus.haltmeier@uibk.ac.at`

Abstract. Increasing the imaging speed is a central aim in photoacoustic tomography. In this work we address this issue using techniques of compressed sensing. We demonstrate that the number of measurements can significantly be reduced by allowing general linear measurements instead of point wise pressure values. A main requirement in compressed sensing is the sparsity of the unknowns to be recovered. For that purpose we develop the concept of sparsifying temporal transforms for three dimensional photoacoustic tomography. Reconstruction results for simulated and for experimental data verify that the proposed compressed sensing scheme allows to significantly reducing the number of spatial measurements without reducing the spatial resolution.

PACS numbers: 43.35.Ud, 87.85.Ng, 43.38.Zp

Keywords: Photoacoustic tomography, optoacoustic imaging, compressed sensing, sparsity, non-contact photoacoustic imaging

1. Introduction

Photoacoustic tomography (PAT), also known as optoacoustic tomography, is a novel non-invasive imaging technology that beneficial combines the high contrast of pure optical imaging with the high spatial resolution of pure ultrasound imaging (see [1, 2, 3]). The basic principle of PAT is as follows. A semitransparent sample (such as a part of a human patient) is illuminated with short pulses of optical radiation. A fraction of the optical energy is absorbed inside the sample which causes thermal heating, expansion, and a subsequent acoustic pressure wave depending on the interior absorbing structure of the sample. The acoustic pressure is measured outside of the sample and used to reconstruct an image of the interior.

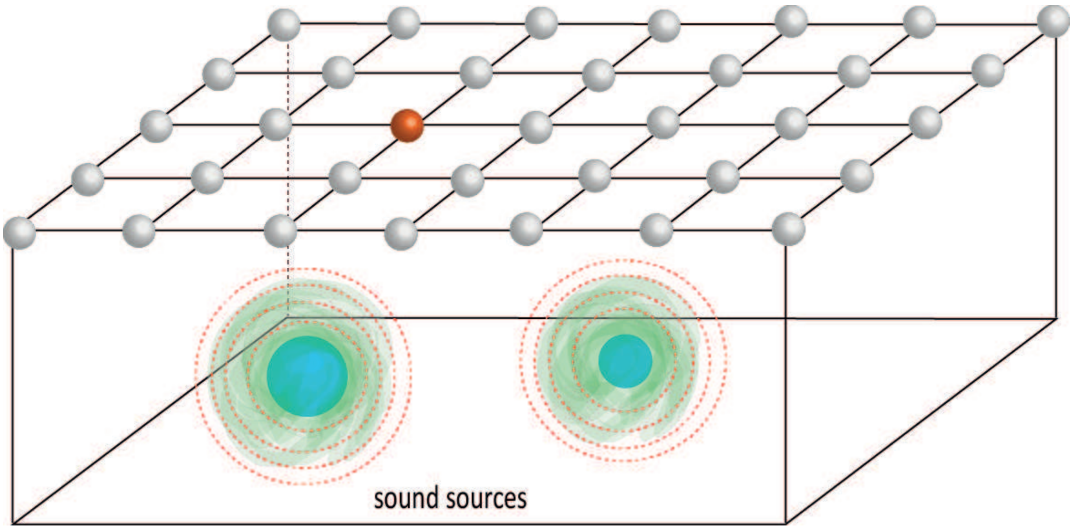

Figure 1. BASIC SETUP OF PAT. An object is illuminated with a short optical pulse that induces an acoustic pressure wave. The pressure wave is measured on a surface and used to reconstruct an image of the interior absorbing structure.

The standard sensing approach in PAT is to measure the acoustic pressure with small detector elements distributed on a surface outside of the sample; see Figure 2. The spatial sampling step size determines the resolution of the pressure data and the resolution of the final reconstruction. Consequently, high spatial resolution requires a large number of detector locations. Ideally, for high frame rate, the pressure data are measured in parallel with a large array made of small detector elements. However, the signal-to-noise ratio and therefore the sensitivity decreases for smaller detector elements and producing a large array with high bandwidth is costly and difficult to fabricate. Therefore, often a single detector element (or a small number of such) is used to record the acoustic pressure. In order to collect sufficient data the measurement process has to be repeated with changed locations of the detector elements. Obviously, such an approach slows down the imaging speed. As an alternative to the usually employed piezoelectric transducers, optical detection schemes have been used to acquire the pressure data on the surface of samples [4, 5, 6, 7]. In these methods an optical beam is raster scanned along a surface and the pressure data are recorded at the location of the interrogation beam.

In order to keep the sensitivity high, to reduce production costs, and to increase the imaging speed one has to reduce the number of spatial measurements. For that purpose, we develop a compressed sensing scheme for three dimensional PAT using a planar measurement geometry.

1.1. Compressed sensing

Compressed sensing (or compressive sampling) is a new sensing paradigm introduced recently in [8, 9, 10]. It allows to capture high resolution signals using much less measurements than advised by Shannon's sampling theory. The basic idea in compressed sensing is replacing point measurements by general linear measurements, where each measurements consist of a linear combination

$$\mathbf{y}[j] = \sum_{i=1}^{n} \mathbf{A}[j,i]\mathbf{x}[i] \quad \text{for } j = 1, \dots, m\,. \tag{1}$$

Here $\mathbf{x}$ is the desired high resolution signal (or image), $\mathbf{y}$ the measurement vector, and $\mathbf{A}$ the measurement matrix. If $m \ll n$, then (1) is a severely under-determinated system of linear equations for the unknown signal. The theory of compressed sensing predicts that under suitable assumptions the unknown signal can nevertheless be stably recovered from such data.

The crucial ingredients of compressed sensing are sparsity and randomness.

(i) SPARSITY: This refers to the requirement that the unknown signal is sparse, in the sense that it has only a small number of entries that are significantly different from zero (possibly after a change of basis).

(ii) RANDOMNESS: This refers to selecting the entries of the measurement matrix in a certain random fashion. This guarantees that the measurement data are able to sufficiently well separate sparse vectors.

In this work we use randomness and sparsity to develop compressed sensing techniques for three dimensional PAT. For that purpose we simplify and extend the concept of sparsifying transforms originally introduced in [11, 12] for PAT with integrating line detectors.

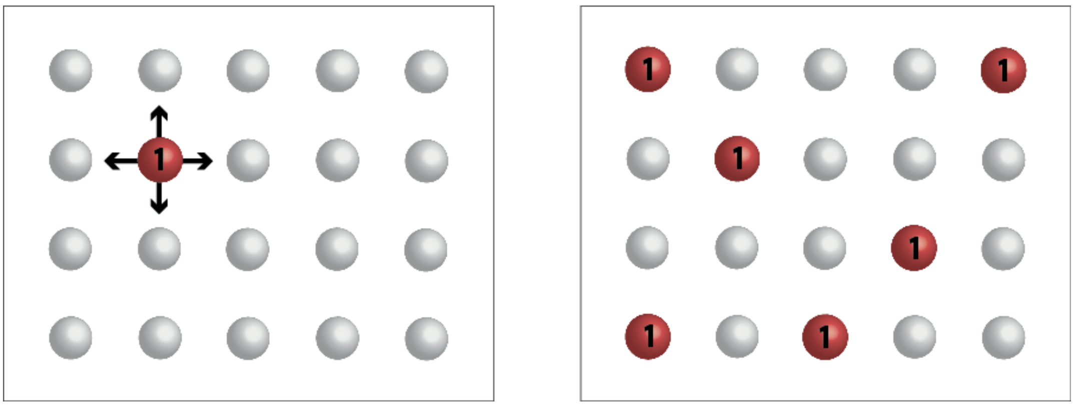

Figure 2. STANDARD SAMPLING VERSUS COMPRESSED SENSING. Left: Standard sampling records point-wise data at individual detector positions. Right: Compressed sensing measurements consist of random combinations of point-wise data values.

1.2. Compressed sensing and sparsity in PAT

In PAT, temporal samples can easily be collected at a high rate compared to spatial sampling, where each sample requires a separate sensor. It is therefore natural to work with semi-discrete data $p(\mathbf{r}_S[i], \cdot\,)$, where $\mathbf{r}_S[i]$ denote locations on the detection surface. Compressed sensing measurements in PAT consist of linear combinations

$$\mathbf{y}[j, \cdot\,] = \sum_{i=1}^{n} \mathbf{A}[j,i]\, p(\mathbf{r}_S[i], \cdot\,) \quad \text{for } j \in \{1, \ldots, m\}\,. \tag{2}$$

Here $m \ll n$ is the number of measurements and $\mathbf{A}$ the $m \times n$ measurement matrix. In PAT (as in many other imaging applications) arbitrary matrix entries are difficult to be realized. It is most simple to use binary combinations of pressure values, where $\mathbf{A}[j,i]$ only takes two values (state on and state off). In this work we restrict ourselves to such a situation. In the PAT literature two types of binary compressed sensing matrices have been proposed. In [13, 14] scrambled Hadamard matrices have been used. In [11, 12] measurements matrices are taken as the adjacency matrix of a left d-regular bipartite graph, where the measurement matrix is sparse and has exactly d ones in each column, whose locations are randomly selected. In both cases, the random nature of the selected coefficients yields compressed sensing capability the measurement matrix.

Sparsity of the signal to be recovered is one of the main ingredients of compressed sensing. As in many other applications, sparsity often does not hold in the original domain. Instead sparsity holds in a particular orthonormal basis, such as a wavelet or curvelet basis [15, 16]. In many situations the change of basis destroys the compressed sensing capability of the measurement matrix. In order to overcome this limitation, in [11, 12] we developed the concept of a sparsifying temporal transformation. Such a transform applies in the temporal variable only and results in a filtered pressure signal that is sparse. Because any operation acting in the temporal domain intertwines with the measurement matrix, one can apply sparse recovery to estimate the sparsified pressure. The photoacoustic source can be recovered, in a second step, by applying a standard reconstruction algorithm to the sparsified pressure.

1.3. Outline of this paper

In this paper we develop a compressed sensing scheme based on a sparsifying transform for three dimensional PAT (see Section 3). This complements our work [11, 12], where we introduced the concept of sparsifying transforms for PAT with integrating line detectors. Wave propagation is significantly different in two and in three spatial dimensions. As a result, the sparsifying transform proposed in this work significantly differs from the one presented in [11, 12]. In order to motivate our approach, in Section 2 we provide an introduction to compressed sensing that is required for our PAT compressed sensing approach. In Section 4 we present numerical results on simulated as well as on experimental data from a non-contact photoacoustic imaging setup [17]. These results indicate that the number of spatial measurements can be reduced by at least a factor of

4 compared to the classical point sampling approach. The paper concludes with a short discussion presented in Section 5.

2. Ingredients from compressed sensing

In this section we present the basic ingredients of compressed sensing that are required for understanding its application to PAT. The aim of compressed sensing is to stably recover a signal or image modeled by vector $\mathbf{x} \in \mathbb{R}^n$ from measurements

$$\mathbf{y} = \mathbf{A}\mathbf{x} + \mathbf{e}\,. \tag{3}$$

Here $\mathbf{A} \in \mathbb{R}^{m \times n}$ with $m \ll n$ is the measurement matrix, $\mathbf{e}$ is an unknown error (noise) and $\mathbf{y}$ models the given noisy data. The basic components that make compressed sensing possible are sparsity (or compressibility) of the signal and some form of randomness in the measurement process.

2.1. Sparsity and compressibility

The first basic ingredient of compressed sensing is sparsity, that is defined as follows.

Definition 1 (Sparse signals)**.**
Let $s \in \mathbb{N}$ and $\mathbf{x} \in \mathbb{R}^n$. The vector $\mathbf{x}$ is called s-sparse, if $\|\mathbf{x}\|_0 := \sharp(\{i \in \{1, \dots, n\} \mid \mathbf{x}[i] \neq 0\}) \leq s$. One informally calls $\mathbf{x}$ sparse, if it is s-sparse for sufficiently small s.

In Definition 1, $\sharp(S)$ stands for the number of elements in a set S. Therefore $\|\mathbf{x}\|_0$ counts the number of non-zero entries in the vector $\mathbf{x}$. In the mathematical sense $\|\cdot\|_0$ is neither a norm or a quasi-norm‡ but it is common to call $\|\cdot\|_0$ the ℓ^0-norm. It satisfies $\|x\|_0 = \lim_{p\downarrow 0} \|\mathbf{x}\|_p^p$, where

$$\|\mathbf{x}\|_p := \sqrt[p]{\sum_{i=1}^{n} |\mathbf{x}[i]|^p} \quad \text{with } p > 0 \;\;, \tag{4}$$

stands for the ℓ^p-norm. Recall that $\|\cdot\|_p$ is indeed a norm for $p \geq 1$ and a quasi-norm for $p \in (0, 1)$.

Signals of practical interest are often not sparse in the strict sense, but can be well approximated by sparse vectors. For that purpose we next define the s-term approximation error that can be used as a measure for compressibility.

Definition 2 (Best s-term approximation error)**.**
Let $s \in \mathbb{N}$ and $\mathbf{x} \in \mathbb{R}^n$. One calls

$$\sigma_s(\mathbf{x}) := \inf\{\|\mathbf{x} - \mathbf{x}_s\|_1 \mid \mathbf{x}_s \in \mathbb{R}^n \text{ is } s\text{-sparse}\}$$

the best s-term approximation error of $\mathbf{x}$ (with respect to the ℓ^1-norm).

‡ A quasi-norm satisfies all axioms of a norm, except that the triangle inequality is replaced by the weaker inequality $\|\mathbf{x}_1 + \mathbf{x}_2\| \leq K(\|\mathbf{x}_1\| + \|\mathbf{x}_2\|)$ for some constant $K \geq 1$.

The best s-term approximation error $\sigma_s(\mathbf{x})$ measures, in terms of the ℓ^1-norm, how much the vector $\mathbf{x}$ fails to be s-sparse. One calls $\mathbf{x} \in \mathbb{R}^n$ compressible, if $\sigma_s(\mathbf{x})$ decays sufficiently fast with increasing s. The estimate (see [18])

$$\sigma_s(\mathbf{x}) \leq \frac{q(1-q)^{1/q-1}}{s^{1/q-1}} \|x\|_q \quad \text{for } q \in (0,1) \tag{5}$$

shows that a signal is compressible if its ℓ^q-norm is sufficiently small for some $q < 1$.

2.2. The RIP in compressed sensing

Stable and robust recovery of sparse vectors requires the measurement matrix to well separate sparse vectors. The RIP guarantees such a separation.

Definition 3 (Restricted isometry property (RIP)).
Let $s \in \mathbb{N}$ and $\delta \in (0,1)$. The measurement matrix $\mathbf{A} \in \mathbb{R}^{m \times n}$ is said to satisfy the RIP of order s with constant δ, if, for all s-sparse $\mathbf{x} \in \mathbb{R}^n$,

$$(1-\delta)\|\mathbf{x}\|_2^2 \leq \|\mathbf{A}\mathbf{x}\|_2^2 \leq (1+\delta)\|\mathbf{x}\|_2^2 \,. \tag{6}$$

We write δ_s for the smallest constant satisfying (6).

In the recent years, many sparse recovery results have been derived under various forms of the RIP. Below we give a result derived recently in [19].

Theorem 4 (Sparse recovery under the RIP).
Let $\mathbf{x} \in \mathbb{R}^n$ and let $\mathbf{y} \in \mathbb{R}^m$ satisfy $\|\mathbf{y} - \mathbf{A}\mathbf{x}\|_2 \leq \epsilon$ for some noise level $\epsilon > 0$. Suppose that $\mathbf{A} \in \mathbb{R}^{m \times n}$ satisfies the RIP of order $2s$ with constant $\delta_{2s} < 1/2$, and let $\mathbf{x}_\star$ solve

$$\begin{aligned} &\text{minimize}_{\mathbf{z}} \|\mathbf{z}\|_1 \\ &\text{such that } \|\mathbf{A}\mathbf{z} - \mathbf{y}\|_2 \leq \epsilon \,. \end{aligned} \tag{7}$$

Then, for constants c_1, c_2 only depending on δ_{2s}, $\|\mathbf{x} - \mathbf{x}_\star\|_2 \leq c_1 \sigma_s(\mathbf{x})/\sqrt{s} + c_2\epsilon$.

Proof. See [19]. □

No deterministic construction is known providing large measurement matrices satisfying the RIP. However, several types of random matrices are known to satisfy the RIP with high probability. Therefore, for such measurement matrices, Theorem 4 yields stable and robust recovery using (7). We give two important examples of binary random matrices satisfying the RIP [18].

Example 5 (Bernoulli matrices).
A binary random matrix $\mathbf{B}_{m,n} \in \{-1, 1\}^{m \times n}$ is called Bernoulli matrix if its entries are independent and take the values -1 and 1 with equal probability. A Bernoulli matrix satisfies $\delta_{2s} < \delta$ with probability tending to 1 as $m \to \infty$, if

$$m \geq C_\delta s(\log(n/s) + 1) \tag{8}$$

for some constant $C_\delta > 0$. Consequently, Bernoulli-measurements yield stable and robust recovery by (7) provided that (8) is satisfied.

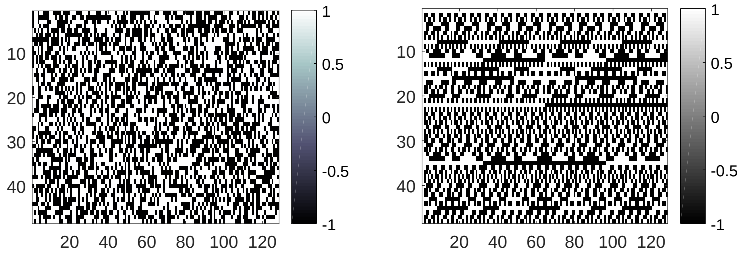

Figure 3. BINARY RANDOM MATRICES SATISFYING THE RIP. Left: Bernoulli matrix is dense and unstructured. Center: Subsampled Hadamard matrix is dense and structured. Right: Sparse adjacency matrix of a left 4-regular bipartite graph.

Bernoulli matrices are dense and unstructured. If n is large then storing and applying such a matrix is expensive. The next example gives a structured binary matrix satisfying the RIP.

Example 6 (Subsampled Hadamard matrices)**.**
Let n be a power of two. The Hadamard matrix $\mathbf{H}_n$ is a binary orthogonal and self-adjoint $n \times n$ matrix that takes values in $\{-1, 1\}$. It can be defined inductively by $\mathbf{H}_1 = 1$ and

$$\mathbf{H}_{2n} := \frac{1}{\sqrt{2}} \begin{bmatrix} \mathbf{H}_n & \mathbf{H}_n \\ \mathbf{H}_n & -\mathbf{H}_n \end{bmatrix} . \tag{9}$$

Equation (9) also serves as the basis for evaluating $\mathbf{H}_n\mathbf{x}$ with $n \log n$ floating point operations. A randomly subsampled Hadamard matrix has the form $\mathbf{P}_{m,n}\mathbf{H}_n \in \{-1, 1\}^{m \times n}$, where $\mathbf{P}_{m,n}$ is a subsampling operator that selects m rows uniformly at random. It satisfies $\delta_{2s} < \delta$ with probability tending to 1 as $n \to \infty$, if

$$m \geq D_\delta s \log(n)^4 \tag{10}$$

for some constant $D_\delta > 0$. Consequently, randomly subsampled Hadamard matrices again yield stable and robust recovery using (7).

2.3. Compressed sensing using lossless expanders

A particularly useful type of binary measurement matrices for compressed sensing are sparse matrices having exactly d ones in each column. Such a measurement matrix can be interpreted as the adjacency matrix of a left d-regular bipartite graph.

Consider the bipartite graph (L, R, E) where $L := \{1, \ldots, n\}$ is the set of left vertices, $R := \{1, \ldots, m\}$ the set of right vertices and $E \subseteq L \times R$ the set of edges. Any element $(i, j) \in E$ can be interpreted as a edge joining vertices i and j. We write

$$N(I) := \{j \in R \mid \exists i \in I \text{ with } (i, j) \in E\}$$

for the set of (right) neighbors of $I \subseteq L$.

Definition 7 (Left d-regular graph)**.**
The bipartite graph (L, R, E) is called d-left regular, if $\sharp[N(\{i\})] = d$ for every $i \in L$.

According to Definition 7, (L, R, E) is left d-regular if any left vertex is connected to exactly d right vertices. Recall that the adjacency matrix $\mathbf{A} \in \{0,1\}^{m \times n}$ of (L, R, E) is defined by $\mathbf{A}[j,i] = 1$ if $(i,j) \in E$ and $\mathbf{A}[j,i] = 0$ if $(i,j) \notin E$. Consequently the adjacency matrix of a d-regular graph contains exactly d ones in each column. If d is small, then the adjacency matrix of a left d-regular bipartite graph is sparse.

Definition 8 (Lossless expander)**.**
Let $s \in \mathbb{N}$ and $\theta \in (0,1)$. A d-left regular graph (L, R, E) is called an (s, d, θ)-lossless expander, if

$$\sharp[N(I)] \geq (1-\theta)\, d\, \sharp[I] \quad \text{for } I \subseteq L \text{ with } \sharp[I] \leq s\,. \tag{11}$$

We write θ_s for the smallest constant satisfying (11).

It is clear that the adjacency matrix of a d-regular graph satisfies $\sharp[N(I)] \leq d\, \sharp[I]$. Hence an expander graph satisfies the two sided estimate $(1-\theta)\, d\, \sharp[I] \leq \sharp[N(I)] \leq d\, \sharp[I]$. Opposed to Bernoulli and subsampled Hadamard matrices, a lossless expander does not satisfy the ℓ^2-based RIP. However, in such a situation, one can use the following alternative recovery result.

Theorem 9 (Sparse recovery for lossless expander)**.**
Let $\mathbf{x} \in \mathbb{R}^n$ and let $\mathbf{y} \in \mathbb{R}^m$ satisfy $\|\mathbf{y} - \mathbf{A}\mathbf{x}\|_1 \leq \epsilon$ for some noise level $\epsilon > 0$. Suppose that $\mathbf{A}$ is the adjacency matrix of a $(2s, d, \theta_{2s})$-lossless expander having $\theta_{2s} < 1/6$ and let $\mathbf{x}_\star$ solve

$$\begin{aligned} &\text{minimize}_{\mathbf{z}} \|\mathbf{z}\|_1 \\ &\text{such that } \|\mathbf{A}\mathbf{z} - \mathbf{y}\|_1 \leq \epsilon\,. \end{aligned} \tag{12}$$

Then, for constants c_1, c_2 only depending on θ_{2s}, we have $\|\mathbf{x} - \mathbf{x}_\star\|_1 \leq c_1 \sigma_s(\mathbf{x}) + c_2 \epsilon / d$.

Proof. See [20, 18]. □

Choosing a d-regular bipartite graph uniformly at random yields a lossless expander with high probability. Therefore, Theorem 9 yields stable and robust recovery for such type of random matrices.

Example 10 (Left d-regular bipartite graphs)**.**
Take $\mathbf{A} \in \{0,1\}^{m \times n}$ as the adjacency matrix of a randomly chosen left d-regular bipartite graph. Then $\mathbf{A}$ has exactly d ones in each column, whose locations are uniformly distributed. Suppose further that for some constant c_θ only depending on θ the parameters d and m have been selected according to

$$\begin{aligned} m &\geq c_\theta s (\log(n/s) + 1) \\ d &= \left\lceil \frac{2\log(n/s) + 2}{\theta} \right\rceil \,. \end{aligned}$$

Then, $\theta_s \leq \theta$ with probability tending to 1 as $n \to \infty$. Consequently, for adjacency matrices of a randomly chosen left d-regular bipartite graphs we have stable and robust recovery by (12).

3. Compressed sensing for PAT in planar geometry

In this section we develop a compressed sensing scheme for PAT, where the acoustic signals are recorded on a planar measurement surface. The planar geometry is of particular interest since it usually can be realized most efficiently in practical applications. We thereby extend the concept of sparsifying temporal transforms introduced for photoacoustic tomography with integrating line detectors in [11, 12].

3.1. PAT in planar geometry

Suppose the photoacoustic source distribution $p_0(\mathbf{r})$ is located in the upper half space $\{(x, y, z) \in \mathbb{R}^3 \mid z > 0\}$. The induced acoustic pressure $p(\mathbf{r}, t)$ satisfies the wave equation

$$\frac{1}{c^2}\frac{\partial^2 p(\mathbf{r},t)}{\partial t^2} - \Delta_{\mathbf{r}} p(\mathbf{r},t) = -\frac{\partial \delta}{\partial t}(t)\, p_0(\mathbf{r})\,, \tag{13}$$

where $\Delta_{\mathbf{r}}$ denotes the spatial Laplacian, $\partial/\partial t$ is the derivative with respect to time, c the sound velocity, and $\delta(t)$ the Dirac delta-function. Here $(\partial\delta/\partial t)p_0$ acts as the sound source at time $t = 0$ and it is supposed that $p(\mathbf{r}, t) = 0$ for $t < 0$. We further denote by

$$(\mathcal{W}p_0)(x_S, y_S, t) := p(x_S, y_S, 0, t)\,,$$

the pressure data restricted to the measurement plane. PAT in planar recording geometry is concerned with reconstructing p_0 from measurements of $\mathcal{W}p_0$.

For recovering p_0 from continuous data explicit and stable inversion formulas, either in the Fourier domain or in the time domain, are well known. A particularly useful inversion method is the universal backprojection (UBP),

$$p_0(\mathbf{r}) = \frac{z}{\pi}\int_{\mathbb{R}^2} \left(t^{-1}\partial_t t^{-1}\mathcal{W}p_0\right)(x_S, y_S, |\mathbf{r} - \mathbf{r}_S|)\,\mathrm{d}S\,. \tag{14}$$

Here $\mathbf{r} = (x, y, z)$ is a reconstruction point, $\mathbf{r}_S = (x_S, y_S, 0)$ a point on the detector surface, and $|\mathbf{r} - \mathbf{r}_S|$ the distance between $\mathbf{r}$ and $\mathbf{r}_S$. The UBP has been derived in [21] for planar, spherical and cylindrical geometry. The two dimensional version of the UBP

$$p_0(\mathbf{r}) = -\frac{2z}{\pi}\int_{\mathbb{R}}\int_{|\mathbf{r}-\mathbf{r}_S|}^{\infty} \frac{(\partial_t t^{-1}\mathcal{W}p_0)(x_S, t)}{\sqrt{t^2 - |\mathbf{r} - \mathbf{r}_S|^2}}\,\mathrm{d}t\mathrm{d}S\,,$$

where $\mathbf{r} = (x, z)$ and $\mathbf{r}_S = (x_S, 0)$ has been first obtained in [22]. In the recent years, the UBP has been generalized to elliptical observation surface in two and three spatial dimensions [23, 24], and various geometries in arbitrary dimension (see [25, 26, 27]).

3.2. Standard sampling approach

In practical application, only a discrete number of spatial measurements can be made. The standard sensing approach in PAT is to distribute detector locations uniformly on a part of the observation surface. Such data can be modeled by

$$\mathbf{p}[i, \cdot\,] := (\mathcal{W}p_0)(x_S[i], y_S[i], \cdot\,) \quad \text{for } i = 1, \ldots, n\,. \tag{15}$$

Temporal samples can easily be collected at a high sampling rate compared to the spatial sampling, where each sample requires a separate sensor. It is therefore natural to consider the semi-discrete data model (15), where the spatial variable is discretized and the temporal variable is kept continuously. The standard UBP algorithm using semi-discrete data consists in discretizing the spatial integral in (14) using a discrete sum over all detector locations and evaluating it for a discrete number of reconstruction points. This yields to the following UBP reconstruction algorithm.

Algorithm 1 (UBP algorithm for PAT)**.**
Goal: Recover the source p_0 in (13) from data (15).

(S1) Filtration: For any i, t compute $\mathbf{q}[i,t] \leftarrow \partial_t t^{-1} \partial_t t^{-1} \mathbf{p}[i,t]$.

(S2) Backprojection: For any k set $\mathbf{p}_0[k] \leftarrow v[k]/\pi \sum_{i=1}^{N} \mathbf{q}[i, |\mathbf{r}[k] - \mathbf{r}_S[i]|] w_i$.

In Algorithm 1, the first step (S1) can be interpreted as temporal filtering operation. The second step (S2) discretizes the spatial integral in (14) and is called discrete backprojection. The numbers w_i are weights for the numerical integration and account for density of the detector elements. Note that an analogous reconstruction algorithm can be obtained for two spatial dimensions by implementing the two dimensional UBP formula.

3.3. Compressed sensing approach

Performing a large number of spatial measurements is costly and time consuming. In order to speed up the measurement process or to reduce system costs we develop a compressed sensing scheme. Instead of using point-wise samples, compressed sensing measurement performs linear combinations of pressure values,

$$\mathbf{y}[j, \cdot\,] = \sum_{i=1}^{n} \mathbf{A}[j,i]\, \mathbf{p}[i, \cdot\,] \quad \text{for } j \in \{1, \dots, m\}\,. \tag{16}$$

Here $\mathbf{A}$ is the $m \times n$ measurement matrix, and $\mathbf{p}[i,t]$ are point wise pressure data. In the case of compressed sensing we have $m \ll n$, which means that the number of measurements is much smaller than the number of point-samples. In order that the data still captures the essential information one requires the measurement matrix to satisfy certain conditions outlined in the previous section. In PAT (as in many other applications) binary random matrices are most simple to realize. As shown in Section 2 Bernoulli matrices (Example 5), subsampled Hadamard matrices (Example 6) as well as expander graphs (Example 10) can be used for that purpose.

In order to recover the photoacoustic source from compressed sensing data (16), one can use the following two-stage procedure. In the first step we recover the point-wise pressure values from the compressed sensing measurements. In the second step, one applies a standard reconstruction procedure (such as the UBP Algorithm 1) to the estimated point-wise pressure to obtain the photoacoustic source. The first step can be implemented by setting $\hat{\mathbf{p}}[\,\cdot\,,t] := \mathbf{\Psi}\hat{\mathbf{x}}[\,\cdot\,,t]$, where $\hat{\mathbf{x}}[\,\cdot\,,t]$ minimizes the ℓ^1-Tikhonov functional

$$\|\mathbf{y}[\,\cdot\,,t] - \mathbf{A}\mathbf{\Psi}\mathbf{x}\|^2 + \|\mathbf{x}\|_1\,. \tag{17}$$

Here $\mathbf{\Psi} \in \mathbb{R}^{n\times n}$ is a suitable basis (such as orthonormal wavelets) that sparsely represents the pressure data and λ is a regularization parameter. Note that (17) can be solved separately for every $t \in [0,T]$ which makes the two stage approach particularly efficient. The resulting two-stage reconstruction scheme is summarized in Algorithm 2.

Algorithm 2 (Two-stage compressed sensing reconstruction scheme)**.**
Goal: Recover p_0 from data (16).

(S1) Recovery of point-measurements:
- Choose a sparsifying basis $\mathbf{\Psi} \in \mathbb{R}^{n\times n}$.
- For every t, find an approximation $\hat{\mathbf{p}}[\,\cdot\,,t] := \mathbf{\Psi}\hat{\mathbf{x}}[\,\cdot\,,t]$ by minimizing (17).

(S2) Recover p_0 by applying a PAT standard reconstruction algorithm to $\hat{\mathbf{p}}[\,\cdot\,,t]$.

As an alternative to the proposed two-stage procedure, the photoacoustic source could be recovered directly from data (16) based on minimizing the ℓ^1-Tikhonov regularization functional [28, 29]

$$\frac{1}{2}\|(\mathbf{A}\circ\mathcal{W})\hat{p}_0\|_2^2 + \lambda\|\mathbf{\Psi}\hat{p}_0\|_1 \to \min_{\hat{p}_0}\,. \tag{18}$$

Here $\mathbf{\Psi}$ is suitable basis that sparsifies the photoacoustic source p_0. However, such an approach is numerically expensive since the wave equation and its adjoint have to be solved repeatedly. The proposed two-step reconstruction scheme is much faster because it avoids evaluating the wave equation, and the iterative reconstruction decouples into lower dimensional problems for every t. A simple estimation of the number of floating point operations (flops) reveals the dramatic speed improvement. Suppose we have $n = N \times N$ detector locations, $\mathcal{O}(N)$ time instance and recover the source on a $N \times N \times N$ spatial grid. Evaluation of a straight forward time domain discretization of $\mathcal{W}$ and its adjoint require $\mathcal{O}(N^5)$ flops. Hence, the iterative one-step reconstruction requires $N_{\mathrm{iter}}\,\mathcal{O}(N^5)$ operations, where N_{iter} is the number of iterations. On the other hand the two-stage reconstruction requires $N_{\mathrm{iter}}\mathcal{O}(N^3m)$ flops for the iterative data completion and additionally $\mathcal{O}(N^5)$ flops for the subsequent UBP reconstruction. In the implementation one takes the number of iterations (at least) in the order of N and therefore the two-step procedure is faster by at least one order of magnitude.

3.4. Sparsifying temporal transform

In order that the pressure data can be recovered by (17) one requires a suitable basis $\mathbf{\Psi} \in \mathbb{R}^{n\times n}$ such that the pressure is sparsely represented in this basis and that the composition $\mathbf{A} \circ \mathbf{\Psi}$ is a proper compressed sensing matrix. For expander matrices these two conditions are not compatible. To overcome this obstacle in [11, 12] we develop the concept of a sparsifying temporal transform for the two dimensional case in circular geometry. Below we extend this concept to three spatial dimensions using combinations of point-wise pressure values.

Suppose we apply a transformation $\mathbf{T}$ to the data $t \mapsto \mathbf{y}[\,\cdot\,, t]$ that only acts in the temporal variable. Because the measurement matrix $\mathbf{A}$ is applied in the spatial variable, the transformation $\mathbf{T}$ and the measurement matrix commute, which yields

$$\mathbf{Ty} = \mathbf{A}(\mathbf{Tp})\,. \tag{19}$$

We call $\mathbf{T}$ a sparsifying temporal transform, if $\mathbf{Tp}[\,\cdot\,, t] \in \mathbb{R}^n$ is sufficiently sparse for a suitable class of source distributions and all times t. In this work we propose the following sparsifying spatial transform

$$\mathbf{T}(\mathbf{p}) := t^3 \partial_t t^{-1} \partial_t t^{-1} \mathbf{p}\,. \tag{20}$$

The sparsifying effect of this transform is illustrated in Figure 4 applied to the pressure data arising from a uniform spherical source; see also Theorem 11 in the Appendix for a rigorous estimate.

Having a sparsifying temporal transform at hand, we can construct the photoacoustic source by the following modified two-stage approach. In the first step recover an approximation $\hat{\mathbf{q}}[\,\cdot\,, t] \simeq \mathbf{Tp}[\,\cdot\,, t]$ by solving

$$\frac{1}{2}\|\mathbf{Ty}[\,\cdot\,, t] - \mathbf{A}\hat{\mathbf{q}}[\,\cdot\,, t]\|^2 + \|\hat{\mathbf{q}}[\,\cdot\,, t]\|_1 \to \min_{\hat{\mathbf{q}}}\,. \tag{21}$$

In the second step, we recover the photoacoustic source by implementing the UBP expressed in terms of the sparsified pressure,

$$p_0(\mathbf{r}) = -\frac{z}{\pi}\int_{\mathbb{R}^2}\int_{|\mathbf{r}-\mathbf{r}_S|}^{\infty} (t^{-3}\mathbf{T}\mathcal{W}p_0)(x_S, y_S, t)\,\mathrm{d}t\mathrm{d}S\,. \tag{22}$$

Here $\mathbf{r} = (x, y, z)$ is a reconstruction point and $\mathbf{r}_S = (x_S, y_S, 0)$ a point on the measurement surface. The modified UBP formula (22) can be implemented analogously to Algorithm 1. In summary, we obtain the following reconstruction algorithm.

Algorithm 3 (Compressed sensing reconstruction with sparsifying temporal transform)**.**
Goal: Reconstruct p_0 in (13) from data (16).

(S1) Recover sparsified point-measurements:
- Compute the filtered data $\mathbf{Ty}(t)$
- Recover an approximation $\hat{\mathbf{q}}[\,\cdot\,, t]$ to $\mathbf{Tp}[\,\cdot\,, t]$ by solving (21).

(S2) UBP algorithm for sparsified data:
- For any i, ρ set $\mathbf{q}[i, \rho] \leftarrow \int_\rho^\infty t^{-3}\mathbf{q}[i, t]\,\mathrm{d}t$
- For any k set $p_0[k] \leftarrow \frac{v[k]}{\pi}\sum_{i=1}^N \mathbf{q}[i, |\mathbf{r}[k] - \mathbf{r}_S[i]|]w_i$.

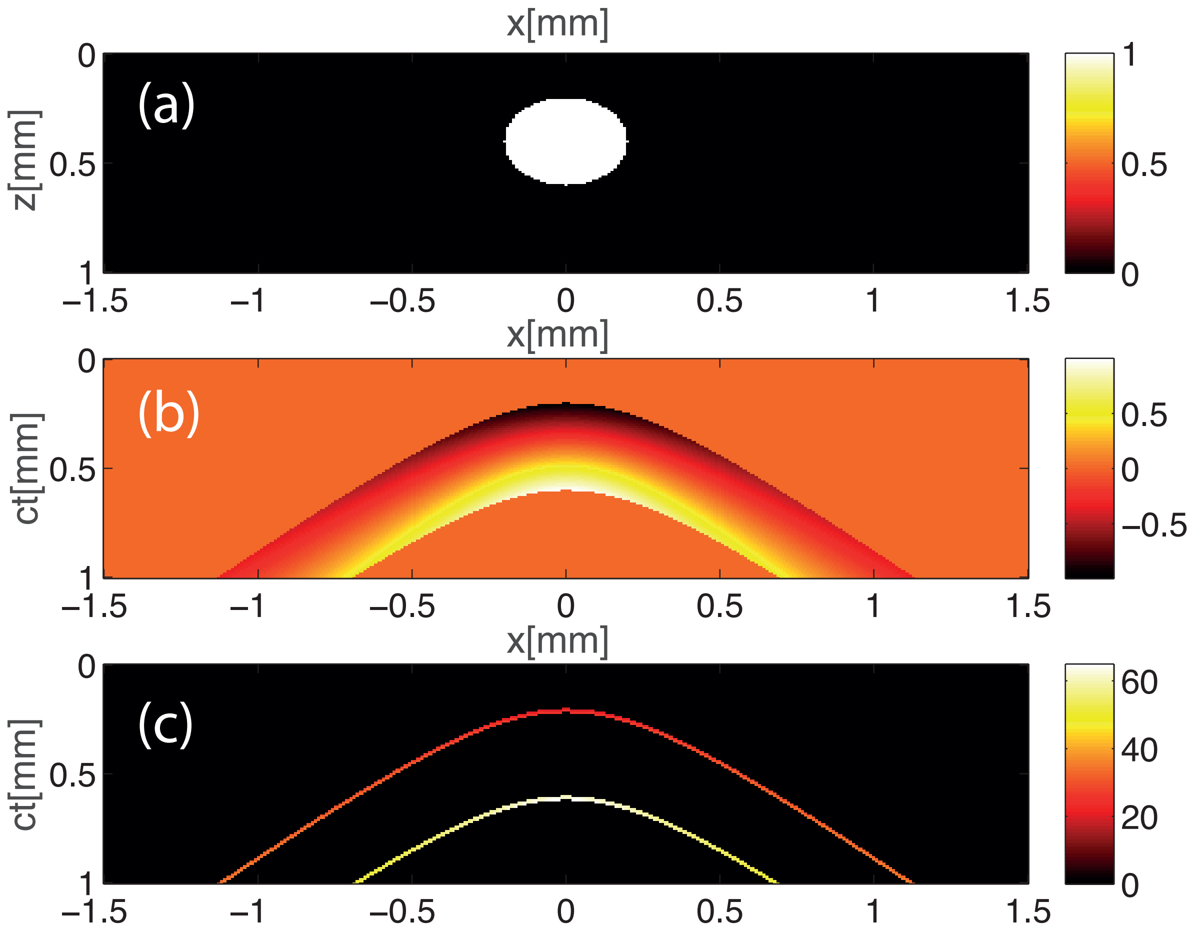

Figure 4. Effect of the sparsifying transform. Top: Cross section of a uniform spherical source. Middle: Corresponding pressure data. Bottom: Result after applying the sparsifying transform $\mathbf{T}$.

Since (21) can be solved separately for every t, the modified two-stage Algorithm 3 is again much faster than a direct approach based on (18). Moreover, from general recovery results in compressed sensing presented in the previous section Algorithm 3 yields theoretical recovery guarantees for Bernoulli, subsampled Hadamard matrices as well as adjacency matrices of left d-regular graphs (see Figure 3).

4. Numerical and experimental results

4.1. Simulated data

We consider reconstructing a superposition of two spherical absorbers, having centers in the vertical plane $\{(x, y, z) \in \mathbb{R}^3 \mid y = 0\}$. The vertical cross section of the photoacoustic source is shown in Figure 5(a). In order to test our compressed sensing approach we first create point samples of the pressure $\mathcal{W}p_0$ on an equidistant Cartesian grid on the square $[-3, 3] \times [-3, 3]$ using 64×64 grid points. From that we compute compressed

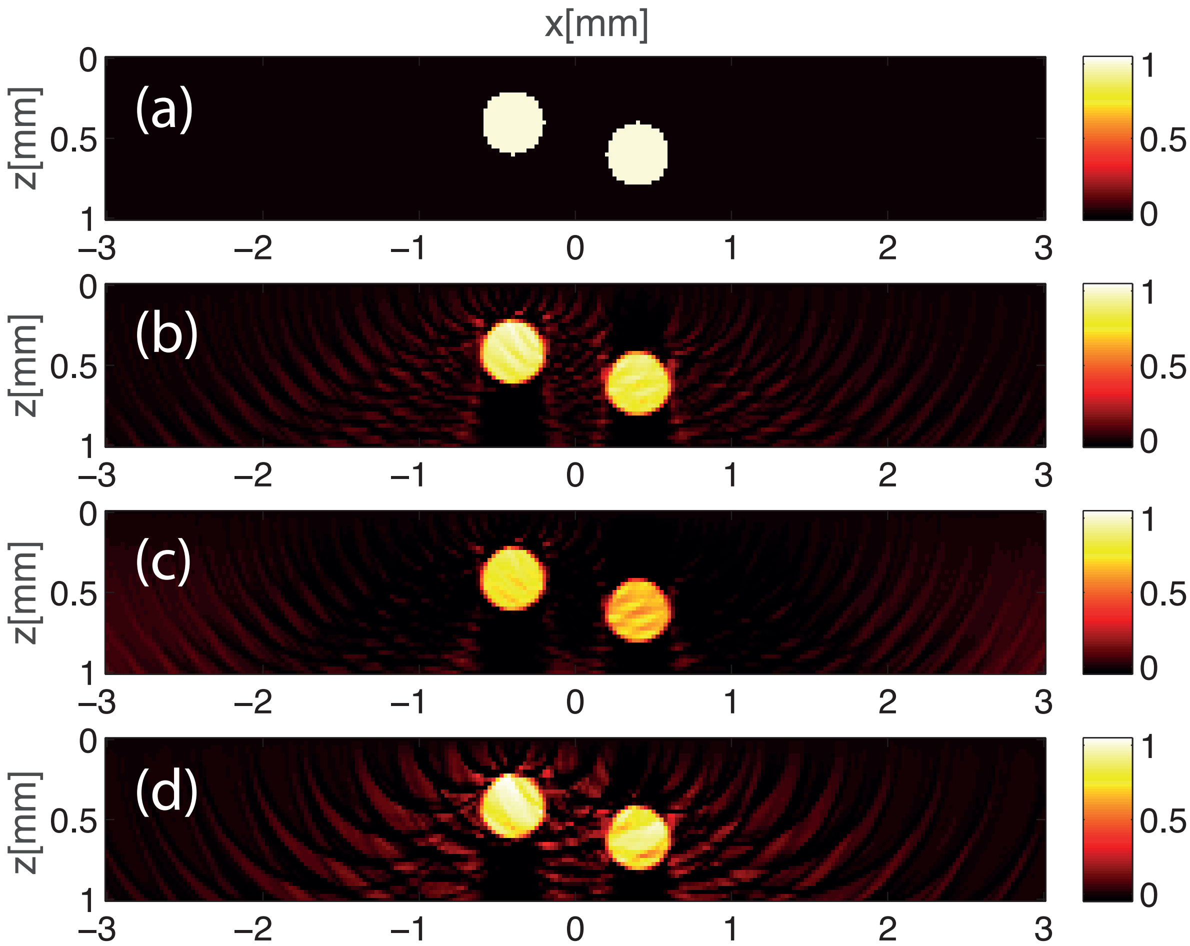

Figure 5. Three dimensional compressed sensing PAT versus standard approach. (a) Cross section of superposition of two uniform spherical absorbers. (b) Reconstruction using 4096 point measurements on a Cartesian grid. (c) Compressed sensing reconstruction using 1024 measurements with $d = 15$. (d) Reconstruction using 1024 point measurements on a Cartesian grid.

sensing data

$$\mathbf{y}[j,t] = \sum_{i=1}^{4096} \mathbf{A}[j,i]\mathbf{p}[i,t] \quad \text{for } j \in \{1,\ldots,1024\}\,. \tag{23}$$

The choice $m = 1024$ corresponds to an reduction of measurements by a factor 4. The matrix $\mathbf{A}$ was chosen as the adjacency matrix of a randomly left d-regular graph with $d = 15$; see Example 11.

Figure 5 shows the reconstruction results using 4096 point samples using Algorithm 1 (Figure 5(b)) and the reconstruction from 1024 compressed sensing measurements using Algorithm 3 (Figure 5(c)). The ℓ^1-minimization problem (21) has been solved using the FISTA [30]. We see that the image quality from the compressed sensing reconstruction is comparable to the reconstruction from full data using only a fourth of the number of measurements. For comparison purpose, Figure 5(d) also shows the reconstruction using 1024 point samples. One clearly recognizes the increase of

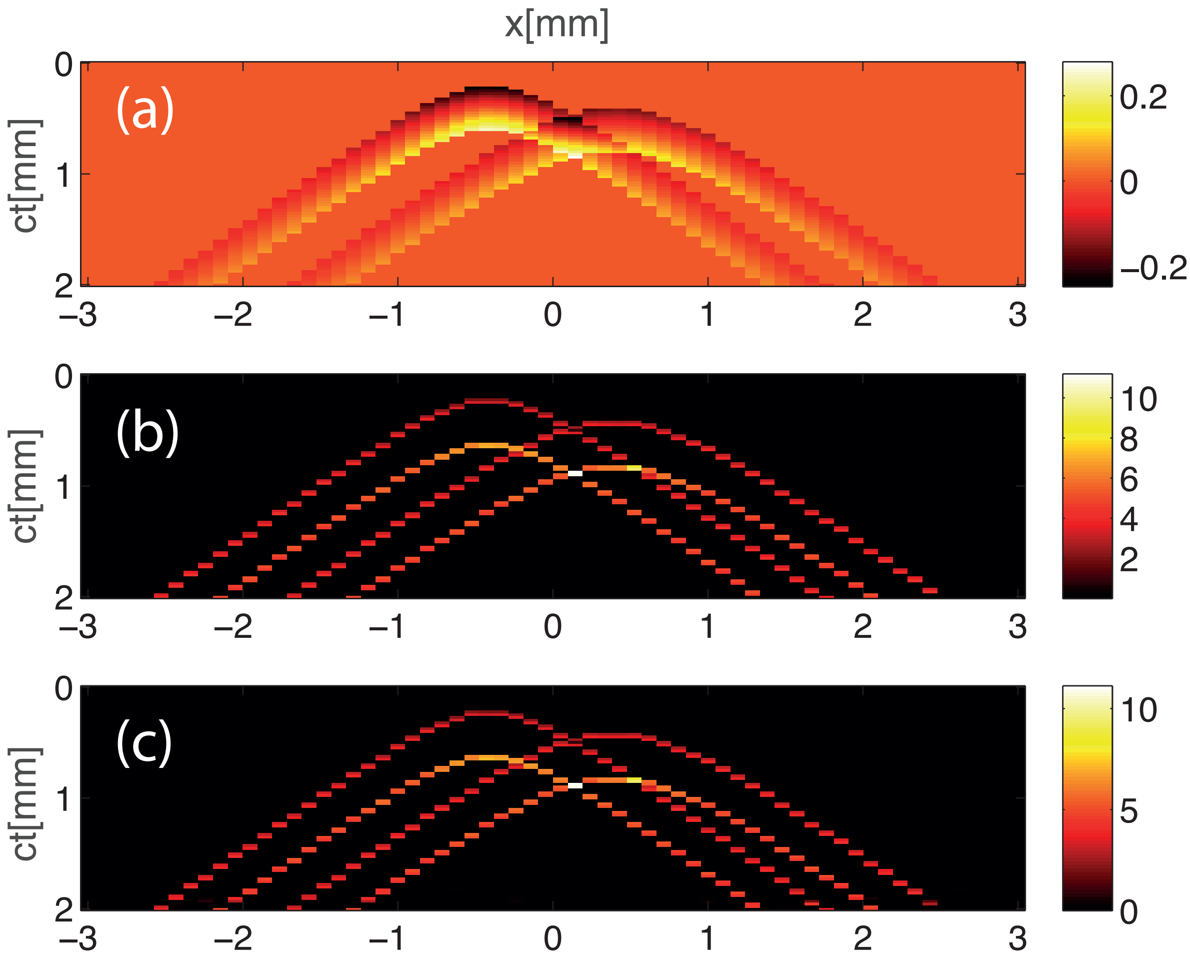

Figure 6. Result of sparse recovery. (a) Pressure at $z = 0$ induced by two spherical absorbers shown in Figure 5. (b) Result after applying the sparsifying transform. (c) Reconstruction of the sparsified pressure from compressed sensing measurements using ℓ^1 minimization.

undersampling artifacts and worse image quality compared to the compressed sensing reconstruction using the same number of measurements. Figure 6 shows the pressure corresponding to the absorbers shown in Figure 5 together with the sparsified pressure and its reconstruction from compressed sensing data.

4.2. Results for real measurement data

Experimental data have been obtained from a silicone tube phantom as shown in Figure 7. The silicone tube was filled with black ink, formed to a knot, and immersed in a milk/water emulsion. The outer and inner diameters of the tube were 600 μm and 300 μm, respectively. Milk was diluted into the water to mimic the optical scattering properties of tissue; an adhesive tape, placed on the top of the water/milk emulsion, was used to mimic skin. Photoacoustic signals were excited with nanosecond pulses from an optical parametric oscillator pumped by a frequency doubled Nd:YAG laser.

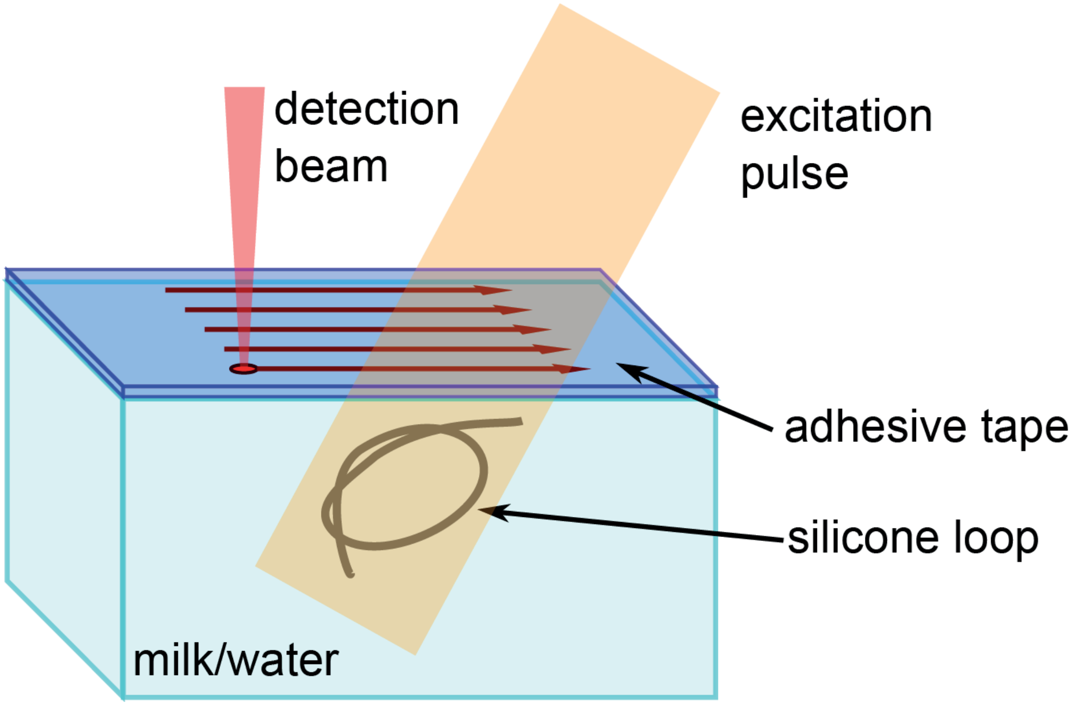

Figure 7. Schematic of experimental setup of non-contact photoacoustic imaging. Photoacoustic waves are excited by short laser pulses. The ultrasonic signals are measured on the surface of the sample using a non-contact photoacoustic imaging technique.

The excitation wavelength was 740 nm. The resulting ultrasonic signals were detected on the adhesive tape by a non-contact photoacoustic imaging setup as described in [17]. In brief, a continuous wave detection beam with a wavelength of 1550 nm was focused onto the sample surface. Displacements on the sample surface, generated by the impinging ultrasonic waves, change the phase of the reflected laser beam. By collecting and demodulating the reflected light, the phase information and, thus, information on the ultrasonic displacements at the position of the laser beam can be obtained. To allow three-dimensional measurements, the detection beam is raster scanned along the surface.

Using this setup, point-wise pressure data on the measurement surface have been collected for $4331 = 71 \times 61$ detector positions on the measurement plane. From this data we generated $m = 1116$ compressed sensing measurements, where each detector location has been used $d = 10$ times in total. Figure 8 shows the maximum amplitude projections along the z, x, and y-direction, respectively, of the three dimensional reconstruction from compressed sensing data using Algorithm 3. The sparsified pressure has been reconstructed by minimizing (21) with the FISTA. For comparison purpose, in Figure 9 we show the maximum amplitude projections from the UBP Algorithm 1 applied to the original data set. We observe that there is only a small difference between the reconstruction results. However the compressed sensing approach uses only a fourth of the number of measurements of the original data set. This clearly demonstrates the potential of our compressed sensing scheme for decreasing the number of measurements while keeping the image quality.

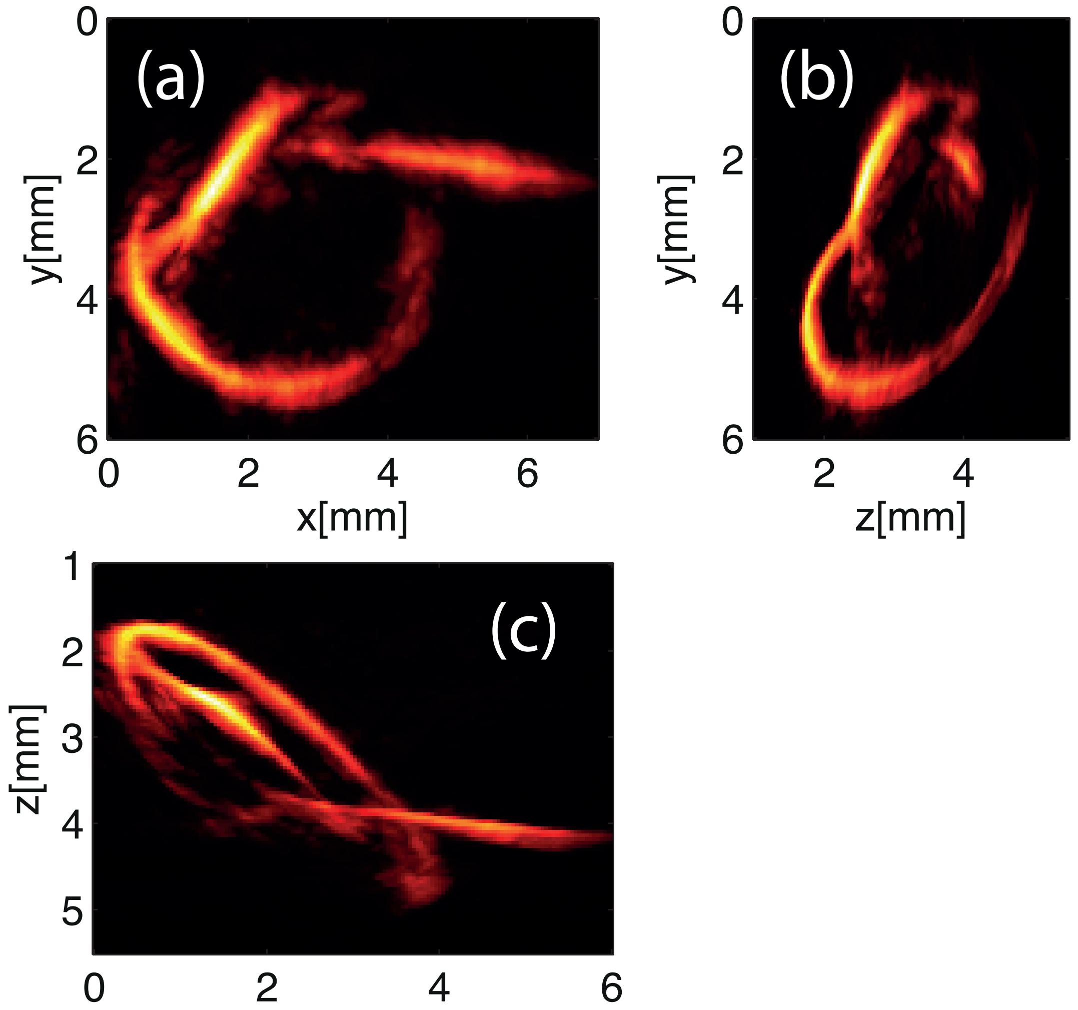

Figure 8. Reconstruction results using compressed sensing measurements. Maximum intensity projections of a silicone loop along the z-direction (a), the x-direction (b), and the y-direction (c).

5. Conclusion and outlook

To speed up the data collection process in PAT while keeping sensitivity high and production costs low, one has to reduce the number of spatial measurements. In this paper we proposed a compressed sensing scheme for that purpose using random measurements in combination with a sparsifying temporal transform. We presented a selected review of compressed sensing that demonstrates the role of sparsity and randomness for high resolution recovery. Using general results from compressed sensing we were able to derive theoretical recovery guarantees for our approach based on sparsifying temporal transforms. Further, this comes with a fast algorithmic

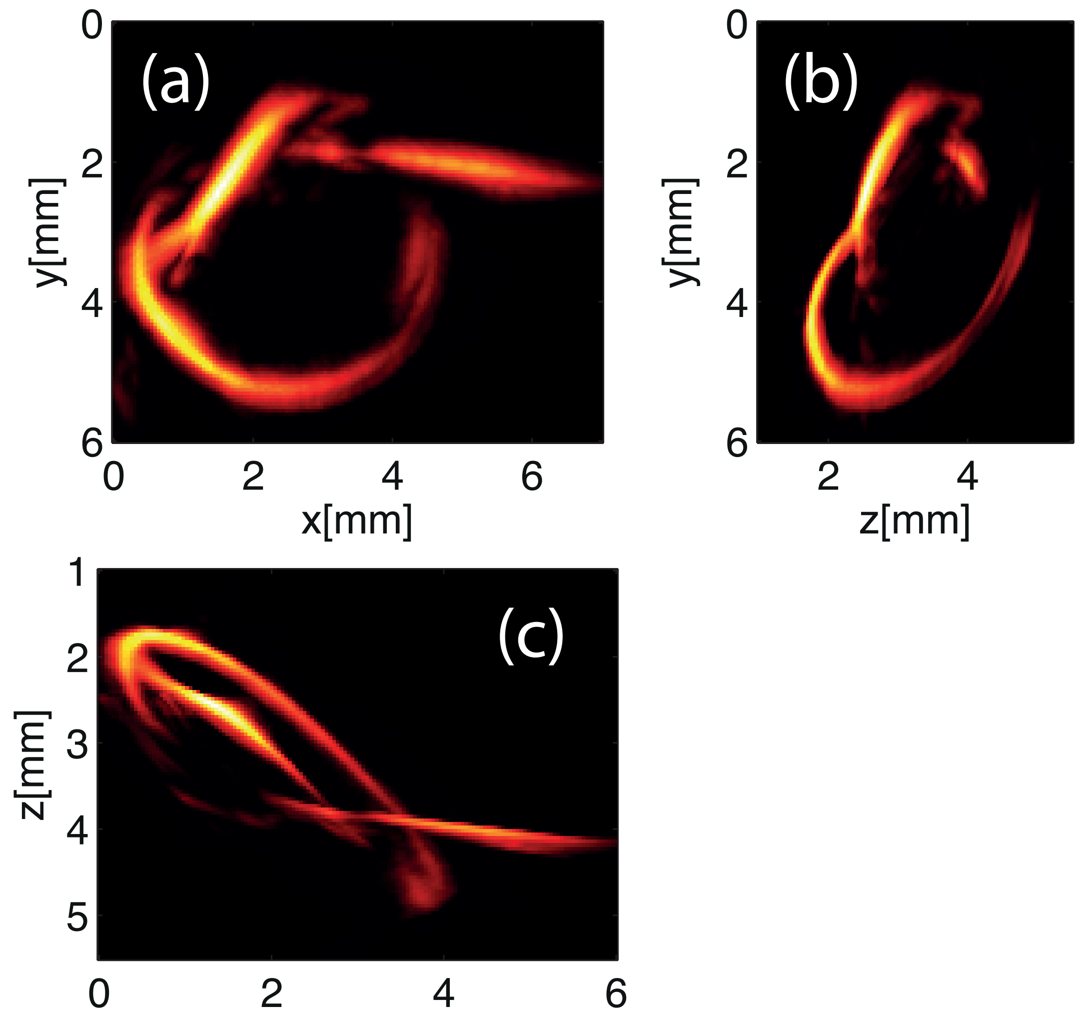

Figure 9. Reconstruction results using full measurements. Maximum intensity projections of a silicone loop along the z-direction (a), the x-direction (b), and the y-direction (c).

implementation. Compressed sensing schemes without using random measurements and with much slower algorithmic realization have been considered in [31, 32].

Acknowledgments

This work has been supported by the Austrian Science Fund (FWF), project number P25584-N20, the Christian Doppler Research Association (Christian Doppler Laboratory for Photoacoustic Imaging and Laser Ultrasonics), the European Regional Development Fund (EFRE) in the framework of the EU-program Regio 13, the federal state Upper Austria. S. Moon thanks University of Innsbruck for its hospitality during his visit. The work of S. Moon has been supported by the National Research Foundation of Korea grant funded by the Korea government (MSIP) (2015R1C1A1A01051674) and the TJ Park Science Fellowship of POSCO TJ Park Foundation.

Appendix A. Compressibility of the pressure signals

In this appendix we present a rigorous mathematical result that justifies the proposed sparsifying transform. For the sake of clarity we consider a spherical photoacoustic absorber that takes the value a_0 for $|\mathbf{r}-\mathbf{m}| \leq R$ and zero otherwise. Here $\mathbf{m} = (0,0,1)$ is the center, R the radius and a_0 the amplitude of the source. The induced acoustic pressure of such a spherical absorber is given

$$p(\mathbf{r}_S, t) = \frac{a_0}{2} \begin{cases} \frac{t-|\mathbf{r}_S-\mathbf{m}|}{|\mathbf{r}_S-\mathbf{m}|} & \text{if } |t-|\mathbf{r}_S-\mathbf{m}|| \leq R \\ 0 & \text{otherwise}\,. \end{cases}$$

For a spatial step size $h > 0$ we consider discrete samples of the pressure evaluated at $\mathbf{r}_S[i] = (ih, 0, 0)$. In order to avoid spatial undersampling we apply the ideal low-pass filter $H_h(t) := (1/h)\operatorname{sinc}(t\pi/h)$ to the data before sampling. As sparsifying transform we use the slightly modified transform $\mathbf{T}_h = h^2\partial_t^2$.

Theorem 11 (Compressibility of the pressure)**.**
Suppose that $p(\mathbf{r}_S, t)$ is the pressure data generated by a uniform spherical source. Further, for some sampling step size $h \in (0,1]$, denote $H_h(t) := (1/h)\operatorname{sinc}(t\pi/h)$, and consider the semi-discrete data

$$\mathbf{p}[i,\,\cdot\,] := H_h *_t p(ih, 0, 0, \,\cdot\,) \quad \text{for } i = -N, \dots, N\,. \tag{A.1}$$

Then, for any $q \in (1/2, 1)$ the filtered data $\mathbf{T}_h\mathbf{p} := h^2\partial_t^2\mathbf{p}$ satisfy

$$\|\mathbf{T}_h\mathbf{p}[\,\cdot\,, t]\|_q \leq a_0 C_q h^{-1-1/q} \left(1 + \frac{(2q-(N-1)^{1-2q})}{2q-1}\right)^{1/q}, \tag{A.2}$$

where C_q is a constant depending only on q.

The proof of Theorem 11 will be presented elsewhere. Identity (5) and Theorem 11 imply that $\mathbf{T}_h\mathbf{p}[\,\cdot\,, t]$ is compressible in the sense that the best s-term approximation error $\sigma_s(\mathbf{T}_h\mathbf{p}[\,\cdot\,, t])$ is small. Together with Theorem 4 and Theorem 9 this yields stable and robust recovery results for the proposed compressed sensing scheme using $\mathbf{T}_h = h^2\partial_t^2$ as a sparsifying temporal transform.

References

[1] P. Beard. Biomedical photoacoustic imaging. *Interface focus*, 1(4):602–631, 2011.

[2] L. V. Wang. Multiscale photoacoustic microscopy and computed tomography. *Nature Phot.*, 3(9):503–509, 2009.

[3] M. Xu and L. V. Wang. Photoacoustic imaging in biomedicine. *Rev. Sci. Instruments*, 77(4):041101 (22pp), 2006.

[4] E. Zhang, J. Laufer, and P. Beard. Backward-mode multiwavelength photoacoustic scanner using a planar fabry-perot polymer film ultrasound sensor for high-resolution three-dimensional imaging of biological tissues. *Appl. Opt.*, 47(4):561–577, 2008.

[5] T. Berer, A Hochreiner, S. Zamiri, and P Burgholzer. Remote photoacoustic imaging on solid material using a two-wave mixing interferometer. *Opt. Lett.*, 35(24):4151–4153, 2010.

[6] T. Berer, A. Leiss-Holzinger, E. Hochreiner, J. Bauer-Marschallinger, and A. Buchsbaum. Multimodal non-contact photoacoustic and optical coherence tomography imaging using wavelength-division multiplexing. *J. Biomed. Opt.*, 20(4):046013, 2015.

[7] J. Eom, S. Park, and B. B. Lee. Noncontact photoacoustic tomography of in vivo chicken chorioallantoic membrane based on all-fiber heterodyne interferometry. *J. Biomed. Opt.*, 20(4):106007, 2015.

[8] E. J. Candès, J. Romberg, and T. Tao. Robust uncertainty principles: exact signal reconstruction from highly incomplete frequency information. *IEEE Trans. Inf. Theory*, 52(2):489–509, 2006.

[9] E. J. Candès and T. Tao. Near-optimal signal recovery from random projections: universal encoding strategies? *IEEE Trans. Inf. Theory*, 52(12), 2006.

[10] D. L. Donoho. Compressed sensing. *IEEE Trans. Inf. Theory*, 52(4):1289–1306, 2006.

[11] M. Sandbichler, F. Krahmer, T. Berer, P. Burgholzer, and M. Haltmeier. A novel compressed sensing scheme for photoacoustic tomography. *SIAM J. Appl. Math.*, 75(6):2475–2494, 2015.

[12] P. Burgholzer, M. Sandbichler, F. Krahmer, T. Berer, and M. Haltmeier. Sparsifying transformations of photoacoustic signals enabling compressed sensing algorithms. *Proc. SPIE*, 9708:970828–8, 2016.

[13] N. Huynh, E. Zhang, M. Betcke, S. Arridge, P. Beard, and B. Cox. Patterned interrogation scheme for compressed sensing photoacoustic imaging using a fabry perot planar sensor. *Proc. SPIE*, 8943:894327–5, 2014.

[14] N. Huynh, E. Zhang, M. Betcke, S. Arridge, P. Beard, and B. Cox. Single-pixel optical camera for video rate ultrasonic imaging. *Optica*, 3(1):26–29, 2016.

[15] E. Candès, L. Demanet, D. Donoho, and L. Ying. Fast discrete curvelet transforms. *Multiscale Model. Sim.*, 5:861–899, 2006.

[16] S. Mallat. *A wavelet tour of signal processing: The sparse way.* Elsevier/Academic Press, Amsterdam, third edition, 2009.

[17] A. Hochreiner, J. Bauer-Marschallinger, B. Burgholzer, P. Jakoby, and T. Berer. Non-contact photoacoustic imaging using a fiber based interferometer with optical amplification. *Biomed. Opt. Express*, 4(11):2322–2331, 2013.

[18] S. Foucart and H. Rauhut. *A mathematical introduction to compressive sensing.* Springer, 2013.

[19] T. T. Cai and A. Zhang. Sharp RIP bound for sparse signal and low-rank matrix recovery. *Appl. Comput. Harmon. Anal.*, 35(1):74–93, 2013.

[20] R. Berinde, A. C. Gilbert, P. Indyk, H. Karloff, and M. J. Strauss. Combining geometry and combinatorics: A unified approach to sparse signal recovery. In *46th Annual Allerton Conference on Communication, Control, and Computing, 2008*, pages 798–805, 2008.

[21] M. Xu and L. V. Wang. Universal back-projection algorithm for photoacoustic computed tomography. *Phys. Rev. E*, 71(1):016706, 2005.

[22] P. Burgholzer, J. Bauer-Marschallinger, H. Grün, M. Haltmeier, and G. Paltauf. Temporal back-projection algorithms for photoacoustic tomography with integrating line detectors. *Inverse Probl.*, 23(6):S65–S80, 2007.

[23] M. Haltmeier. Inversion of circular means and the wave equation on convex planar domains. *Comput. Math. Appl.*, 65(7):1025–1036, 2013.

[24] F. Natterer. Photo-acoustic inversion in convex domains. *Inverse Probl. Imaging*, 6(2):315–320, 2012.

[25] L. A. Kunyansky. Explicit inversion formulae for the spherical mean Radon transform. *Inverse Probl.*, 23(1):373–383, 2007.

[26] M. Haltmeier. Universal inversion formulas for recovering a function from spherical means. *SIAM J. Math. Anal.*, 46(1):214–232, 2014.

[27] M. Haltmeier and S. Pereverzyev, Jr. The universal back-projection formula for spherical means and the wave equation on certain quadric hypersurfaces. *J. Math. Anal. Appl.*, 429(1):366–382, 2015.

[28] M. Grasmair, M. Haltmeier, and O. Scherzer. Sparse regularization with l^q penalty term. *Inverse Probl.*, 24(5):055020, 13, 2008.

[29] M. Haltmeier. Stable signal reconstruction via ℓ^1-minimization in redundant, non-tight frames. *IEEE Trans. Signal Process.*, 61(2):420–426, 2013.

[30] A. Beck and M. Teboulle. A fast iterative shrinkage-thresholding algorithm for linear inverse problems. *SIAM J. Imaging Sci.*, 2(1):183–202, 2009.

[31] J. Provost and F. Lesage. The application of compressed sensing for photo-acoustic tomography. *IEEE Trans. Med. Imag.*, 28(4):585–594, 2009.

[32] Z. Guo, C. Li, L. Song, and L. V. Wang. Compressed sensing in photoacoustic tomography in vivo. *J. Biomed. Opt.*, 15(2):021311–021311, 2010.